Astron. Astrophys. 319, 617–629 (1997)

ASTRONOMY
AND
ASTROPHYSICS

H_2O^+, CO^+, and dust in Comet P/Swift-Tuttle⋆

K. Jockers[1] **and T. Bonev**[2]

[1] Max-Planck-Institut für Aeronomie, Postfach 20, D-37189 Katlenburg-Lindau, Germany
[2] Institute of Astronomy, Bulgarian Academy of Sciences, Tsarigradsko chaussée 72, 1784 Sofia, Bulgaria

Received 22 March 1996 / Accepted 9 August 1996

Abstract. Comet P/Swift-Tuttle was observed in the light of H_2O^+, CO^+ and continuum with the 2-m telescope of the Bulgarian National Astronomical Observatory (BNAO) on Nov. 25, 1992. We present column density maps of the H_2O^+ and CO^+ ions and a map of the product of filling factor, geometrical albedo, and phase function. The H_2O^+ ions are more concentrated toward the nucleus than CO^+. The ion distributions are in close agreement with magnetohydrodynamic models including photochemistry of H_2O^+, CO^+ and their parents. The color of a spiral dust jet present in the continuum image was redder than the color of the ambient dust. The observations demonstrate the similarity between comets P/Halley and P/Swift-Tuttle.

Key words: comets: general; P/Halley; 109P/Swift-Tuttle

1. Introduction

P/Swift-Tuttle (in the following P/ST) is one of the most remarkable members of the cometary population. It is the first comet which was identified as the parent body of a meteor shower. During the previous apparition of the comet, in 1862, Schiaparelli related P/ST to the Perseids. At that time Winnecke (1864) documented the prominent activity of the comet. Using these drawings Sekanina (1981) modeled the nucleus surface of the comet and found that it must be covered by a large number of active regions.

The last apparition of P/ST, in 1992, added new reasons of interest in this comet. Orbit computations by Marsden (1992) showed that, under certain conditions, the comet may hit the Earth in its next return in 2126. The spectacular dust activity of the comet was confirmed by Yoshida et al. (1993), Boehnhardt & Birkle (1994), and Jorda et al. (1994). Goldberg & Brosh (1995) and Eaton et al. (1995) have shown that the polarization in the jets is higher than in the surroundings. Sanwal et al. (1994) have studied the comet spectrophotometrically and determined the C_2 and CN production rates on four nights in December 1992. Brown et al. (1993) measured velocities of the H_2O^+ flow sunward and tailward of the nucleus of comet P/ST, using high resolution long-slit spectra. A more detailed analysis and interpretation of these measurements was performed by Spinrad et al. (1994).

We observed P/ST with the aim to determine the CO^+ and H_2O^+ contents and their ratio in the near-nucleus region ($< 3\,10^5$ km). These ions are believed to originate in the coma of comets through different mechanisms. The main channel of H_2O^+ generation is photoionization of H_2O and the main loss mechanism for H_2O is photodissociation. The rate constant of photodissociation of H_2O is two orders of magnitude larger than the rate constant of photoionization and therefore determines the extent of the H_2O^+ source region. CO is much more difficult to photodissociate than water. Therefore the CO^+ source is more extended. But CO^+ is not only produced by direct photoionization of CO, but also by dissociative ionization of CO_2 and by an unknown extended source, possibly related to the dust. Ionization by charge exchange with solar wind protons is also more important for CO^+ than for H_2O^+. In the inner coma region, the main ion – neutral reaction channel $CO^+ + H_2O \rightarrow CO + H_2O^+$ (A'Hearn and Festou, 1990) directly decreases the CO^+ to H_2O^+ ratio. Model calculations for comet Halley by Wegmann et al. (1987) show a number density ratio of CO^+ to H_2O^+ less than 1 in the inner coma region and greater than 1 for distances greater than 1.5×10^5 km.

It is therefore of interest to determine observationally the extent of the H_2O^+ and CO^+ comae in comets. The determination of the CO^+ to H_2O^+ ratio allows conclusions about the relative abundance of the most probable parent molecules of both ions, which, on the other hand, can be related to the lifetime of a comet (Cowan & A'Hearn, 1979). More details, related to the origin of the comet or to its evolution can be derived by analyzing the dust distribution and determination of the dust to gas ratio.

2. Observations and reduction

2.1. The instrumentation

Comet P/ST was observed with the 2-m-RCC telescope of the Bulgarian National Astronomical Observatory, Rozhen (BNAO). The focal reducer (FR) of the Max-Planck-Institut for Aeronomy (Jockers,1992) was used with interference fil-

Send offprint requests to: K. Jockers

⋆ Based on observations at the Bulgarian National Astronomical Observatory

Table 1. List of observations of comet P/Swift-Tuttle, Nov 25 1992

No.	UT hh:mm	Filter λ_0, nm	Exposure s	Airmass	Emission
1	16:41	426	300	2.076	CO^+
2	16:53	426	300	2.229	CO^+
3	17:04	642	300	2.411	Continuum
4	17:14	620	300	2.580	H_2O^+
5	17:43	426	300	3.345	CO^+

ters centered at 426 nm, 620nm, and 642 nm for the 0-8-0 $\tilde{A}^2A_1 \rightarrow \tilde{X}^2B_1$ transition of H_2O^+, the (2–0) $A^2\Pi_i \rightarrow X^2\Sigma^+$ transition of CO^+, and for the continuum, respectively. The FR converts the initial focal ratio of f/8 into f/2.8. The interference filters are placed in the parallel beam behind the collimator. Their transmission curves are plotted in Fig. 1, together with portions of comet P/ST spectra, obtained on Nov 17, 1992 by S. Wagner at the 3.5 m telescope of the German-Spanish Astronomical Centre, Calar Alto (M. Küppers, private communication). The dotted line represents a spectrum in the coma of the comet and the dashed one a spectrum about 10^5 km tailward of the nucleus. The CO^+ images are contaminated by a C_3 emission which is confined close to the nucleus. The possible contamination by CH^+ has disappeared in the tailward spectrum because of the relatively short scale length of this ion. More critical is the contamination of the H_2O^+ image by CO^+ emission. If not accounted for, it will cause an overestimate of the H_2O^+ content. In addition, close to the nucleus the H_2O^+ image might be contaminated by C_2 (a blend with CO^+ at 619 nm). The most extended contaminant, C_2, has a scale length of 6.6 10^4 km (A'Hearn et al. 1995) . We therefore will avoid a region of this extent around the nucleus in the discussion of our results.

A camera with an EEV P86000/T CCD chip was employed to record the data. The detector comprises 576 × 385 pixels with size 22 × 22 μ^2. The angular size of the imaged field is 7.0 × 4.6 arcmin with a resolution of 0.8 arcsec per pixel.

2.2. The observations

The observations were carried out in the night of November 25, 1992. A list of the obtained images is given in Table 1. The heliocentric distance of the comet was 1.0 AU, the geocentric distance was 1.3 AU. One pixel equals 756 km at the comet. The deprojected scale along the radius vector of the comet is 1002 km. The phase angle (Earth – comet – Sun) was ≈ 49°.

The spectrophotometric standard star ρ Aql, not far from the location of the comet, was observed for the absolute calibration of the images immediately after the comet frames. Its flux was taken from Voloshina et al. (1982). Intermittent clouds prevented to obtain a sequence of standard stars at different zenith distances.

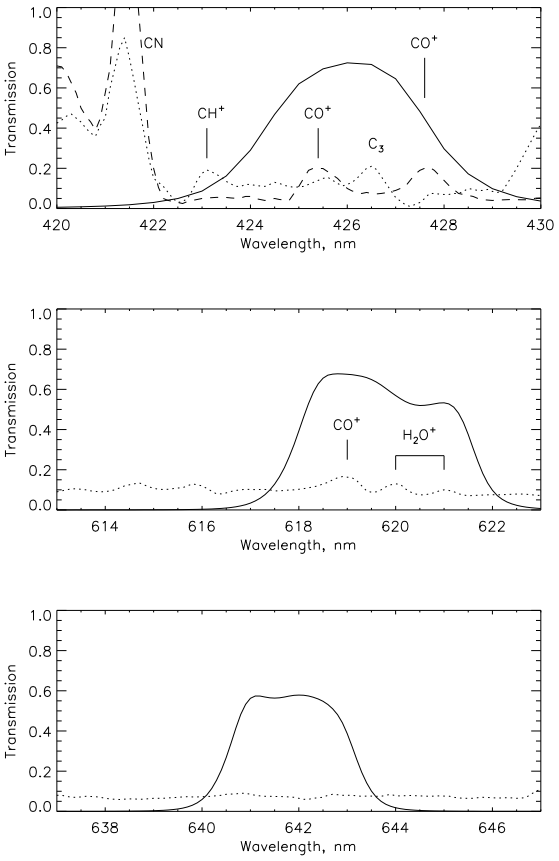

Fig. 1. Transmission curves (solid lines) of the CO^+, H_2O^+, and the continuum filter are shown in the upper, middle, and lower panel. The dotted lines are from a spectrum of comet P/Swift-Tuttle's coma and the dashed line from a tail spectrum.

2.3. Data reduction

2.3.1. Bias, flat fields, and sky background

The raw images were bias subtracted and divided by flat fields, obtained during twilight through the same filters in fall of 1992. As the frame was filled almost entirely by the comet, the process of sky background estimation was somewhat complex. We selected boxes with different sizes in the lower right corner of the images (see Fig. 3). As expected, the histogram analysis of these boxes shows an increasing asymmetry (growing right wing) with increasing boxsize. A rather small box did not contain enough pixels for a statistically significant histogram. A good compromise was found for boxes containing approximately 8000 pixels and having histograms almost symmetrical relative to their maxima. The results of this procedure are summarized in Table 2. The last two columns contain numbers obtained by calculating mean values and standard deviations in several smaller boxes between the star trails in the lower right corner of the images. The numbers in column 2 were adopted as sky background count.

Table 2. Sky background estimation

Image	Histogram analysis Sky, DU	σ_b, DU	Direct measurements Sky, DU	σ_b, DU
1	39	6	38	7
2	38	6	37	6
3	67	4	66	7
4	125	9	123	9
5	28	5	27	6

2.3.2. Extinction correction

For the CO^+ images the extinction coefficient was extracted from the science frames themselves. A value of 0.35 ± 0.005 was obtained by using the total signal in boxes of 10×10 to 70×70 pixel around the nucleus. We consider the obtained value of 0.35 as reliable for several reasons. The first one is the relative large difference between the airmasses at which the three blue images were obtained. Second is the fact that near to the nucleus the signal is dominated by continuum emission (see Fig.2). The independence on box size precludes temporal flux changes of the comet. The third reason is that this value is equal to the mean extinction coefficient for BNAO at this wavelength. For the red spectral region a value of 0.15 was derived from the known ratio of the red to blue extinction coefficients for NAO Rozhen. In order to estimate the photometric error we have considered all standard stars observed with our instrument in a red filter and at λ = 426nm (in total four stars) in October and November 1992 which were observed at similar or better sky conditions and allowed the determination of extinction. The airmasses were 1.01, 1.25, 2.23 and 2.36. The instrument response at λ = 642nm has a standard deviation of $\pm 14\%$ and $\pm 10\%$ at 426 nm. The error in the flux ratio of both wavelength was $\pm 5\%$. A relative error of $\pm 15\%$ for the fluxes and $\pm 5\%$ for the flux ratio seems to be representative for our work.

2.3.3. Subtraction of dust continuum

In order to subtract the continuum from our plasma images we have to obtain a value for the continuum scaling factor, k, defined by the following relation:

$$\text{Emission} = \text{(on-line image)} - k \times \text{(off-line image)} \qquad (1)$$

If neutral color of the cometary dust is assumed, k must be equal to the response ratio of our instrumentation against solar radiation at the wavelengths of the off-line and on-line image. As the standard star used is of A-type we transform to solar fluxes by using the relation:

$$\left(\frac{S_\lambda}{S_{642}}\right)_\odot = \left(\frac{S_\lambda}{S_{642}}\right)_A \times \left(\frac{F_{642}}{F_\lambda}\right)_A \times \left(\frac{F_\lambda}{F_{642}}\right)_\odot , \qquad (2)$$

where S and F are signals and fluxes, respectively, λ indicates the corresponding on-line wavelength, and subscript 'A' stays for the values of the observed A-type star. The fluxes for the sun were taken from the Kurucz atlas (1985) and convolved with the transmission curves of our filters. The numerical values of the different terms appearing in Eq. 2 are presented in Table 3. The k - values in column "neutral" were obtained from the response ratio, $(S_\lambda/S_{642})_\odot$, by performing atmospheric extinction correction for each particular image. The application of "neutral" k-values in Eq. 1 left some residual continuum contribution in the plasma frames. Close to the nucleus the difference images still showed a peak, typical for the continuum. There is theoretical and observational evidence (Bonev and Jockers, 1994) that the plasma distributions are rather flat around the nucleus, whereas the continuum is strongly peaked. Furthermore, the different spatial dependence of the dust tail as compared to the H_2O^+ and CO^+ tails in November 1992 sets another restriction to the determination of the continuum scaling factors. The dust tail has a rather strong curvature toward north (see Fig. 3). Therefore, the choice of the scale factors is limited by the condition that in the upper left corner of the plasma images the ion contribution should be small but must be positive. Another restriction comes from the condition to cancel out the continuum far from the nucleus on its sunward side. Fig. 2 shows profiles parallel to the tail axis averaged over distances from 1.5 to 3 10^4 km northward of nucleus. The signal of the raw on-line image, the intensity scaled off-line image, and their difference, the pure emission, are shown. Evidently, on the sunward side the continuum contributes 90% and more to the total signal in the on-line images. All considered conditions were used as a complex empirical criterion to derive improved values for the continuum scaling factor, k. It turned out to be impossible to simultaneously cancel the overall dust tail and a jet structure close to the nucleus (see Fig. 3). Therefore, with the empirical method two continuum scaling factors were obtained, one for the central peak and one for the dust jet. The values are presented in Table 3 in columns "mean" and "jet", respectively. The continuum contribution in the plasma images was removed by using Eq. (1) with the mean continuum scaling factor (Table 3). The applied criterion allowed the determination of the scaling factors in relativelly narrow limits, about 5% for the CO^+, and 2% for the H_2O^+ image.

In order to increase the signal to noise ratio we removed the star trails from the raw images before performing the continuum subtraction. As the trails are vertical in our images the stars were removed by interactive horizontal interpolation.

2.3.4. Reduction to ion column densities and solar continuum

After continuum subtraction the ion images were calibrated for emission line intensities and then transformed to column densities. Taking into account that we have observed only the red portion of the 0-8-0 transition of H_2O^+ we have taken half of the resonance fluorescence efficiency factor (g-factor) given by Lutz (1987), i.e. $2\,10^{-3}$ photons s^{-1} ion^{-1}. The $A^2\Pi_i \rightarrow X^2\Sigma^+$ (2–0) emission of CO^+ was transformed to column densities by using the g-factor provided by Magnani and A'Hearn (1986). During the observations the heliocentric radial velocity of P/ST

Table 3. Numerical values of the terms in Eq. 2 and the obtained scaling factors for continuum subtraction. See text and Eqs. 1 and 2 for more explanations.

Filter	$\left(\frac{S_\lambda}{S_{642}}\right)_A$	$\left(\frac{F_{642}}{F_\lambda}\right)_A$	$\left(\frac{F_\lambda}{F_{642}}\right)_\odot$	$\left(\frac{S_\lambda}{S_{642}}\right)_\odot$	Continuum scaling factor			Image
					neutral	mean	jet	
IF426	1.68	0.395	1.0565	0.70	0.50	0.45	0.40	1
					0.48	0.43	0.38	2
					0.33	0.30	0.26	5
IF620	1.56	0.927	1.0683	1.54	1.51	1.48	1.48	4

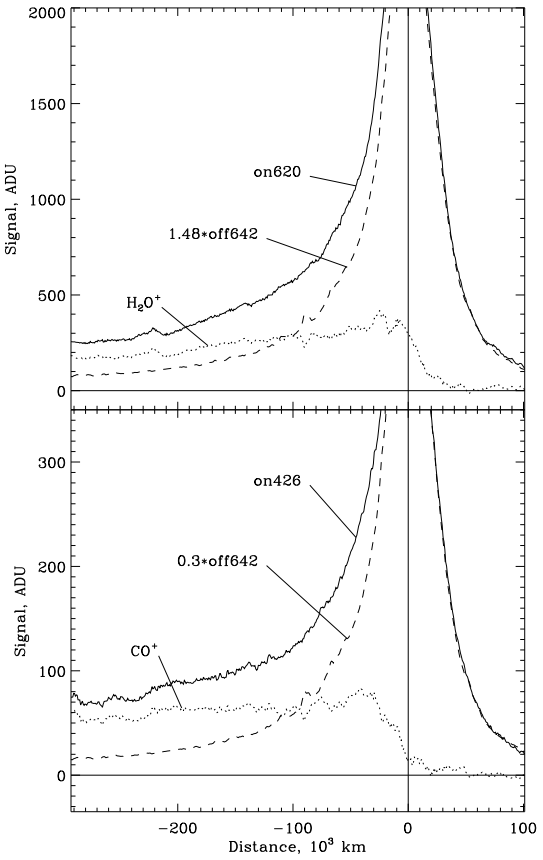

Fig. 2. Upper panel: Signal contributions of H_2O^+ and continuum in the on-line image at 620nm. Lower panel: The same for the CO^+ emission in the on-line image at 426nm. The off-line image is multiplied with the corresponding continuum scaling factors. Cuts are shown parallel to the tail axis. They are averaged over distances from 1.5 to 3 10^4 km northward of nucleus.

was -8.4 km s^{-1}. Most probably further in the tail the ions are accelerated up to velocities, greater than the heliocentric radial velocity of the comet, making thus the influence of the Greenstein effect stronger than that of the Swings effect. Therefore we have taken the g-factor averaged over the values given by Magnani and A'Hearn (1986) for the velocity range +10 - 20 km s^{-1}, 3.7 photons s^{-1} ion^{-1}.

Our H_2O^+-filter is contaminated by the CO^+ $\Pi_{1/2}$ subband of the $A^2\Pi_i \rightarrow X^2\Sigma^+$ (0–2) transition (see Fig. 1). Since we know the CO^+ distribution we can, using the data given by Magnani and A'Hearn (1986), calculate the strength of this contamination and subtract it out. Magnani and A'Hearn do not explicitely tabulate the g-factor for the $\Pi_{1/2}$ subband of the (0–2) transition but within the velocity range 0–50 km s^{-1} it can be calculated from Tables 1 and 2 of this paper to $g = 0.51\ 10^{-3}$ photons s^{-1} ion^{-1}. This leads to a CO^+ contamination in the H_2O^+ filter of $\approx$17%. The H_2O^+ image (Fig. 5) was left uncorrected but in the more quantitative plots of Figs. 6 and 10 this correction was applied.

The continuum image was calibrated in terms of mean solar disk intensities, $i_\odot$ (Jockers et al., 1993). In these units, the continuum intensity, i, is related to the product of geometric albedo, p (Karttunen et al. 1987), phase function, $\Phi(\alpha)$, and filling factor, f, of the dust particles via the equation:

$$p\,\Phi(\alpha)\,f \;=\; \frac{i}{i_\odot}\,\frac{r^2}{R_\odot^2}, \qquad (3)$$

where r is the heliocentric distance of the comet and $R_\odot$ is the solar radius.

3. Results

The calibrated continuum image is shown in Fig. 3. The grey levels present $\log10(p\,\Phi(\alpha)\,f,\ 10^{-8})$. The overplotted contours differ by 1 magnitude. The outermost one belongs to the $3\,\sigma$ level of the background noise and equals about 30% of the sky brightness (see Table 2). The intensity corresponding to the outermost contour is $p\,\Phi(\alpha)\,f = 2.13\,10^{-8}$ which is equivalent to $4.58\ 10^{-13}\,i_\odot$ or to a surface brightness of 19.86 magnitudes arcsec^{-2}. The integration over the whole image yields a brightness of 4.53, in accordance with the light curve of P/ST at this heliocentric distance (Green, 1993). The circumnuclear intensity is dominated by a spiral jet marked in Fig. 3. The area used for sky background determination is indicated.

The three CO^+ and the H_2O^+ images are presented in Figs. 4 and 5, respectively. In both figures the grey scale denotes the column density in 10^{10} ions cm^{-2}. Negative values are seen around the nucleus in the images of both ions. These are artifacts caused by guiding differences between on-line and off-line image. They

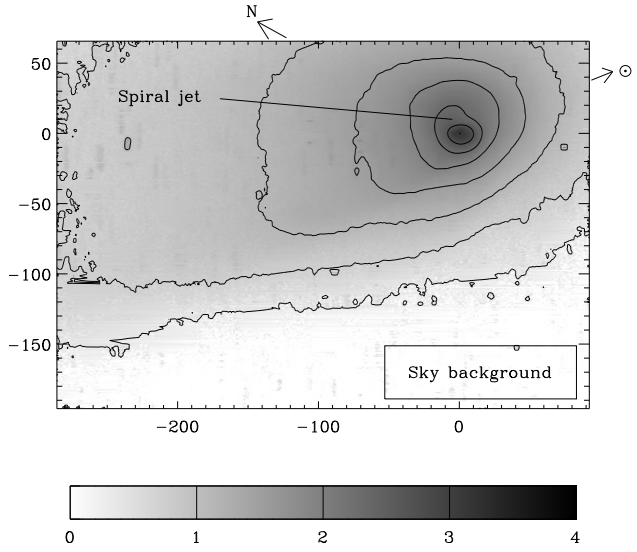

Fig. 3. The continuum image obtained at 642 nm, converted to intensity. The grey levels represent $\log10(p\,\Phi(\alpha)\,f,\ 10^{-8})$. The overplotted contours differ by 1 magnitude and the outermost one denotes an intensity of $p\,\Phi(\alpha)\,f\ =\ 2.13\,10^{-8}$, equivalent to 19.86 magnitudes arcsec^{-2}. The spatial scale is in units of 1000 km at the comet, perpendicular to the line of sight.

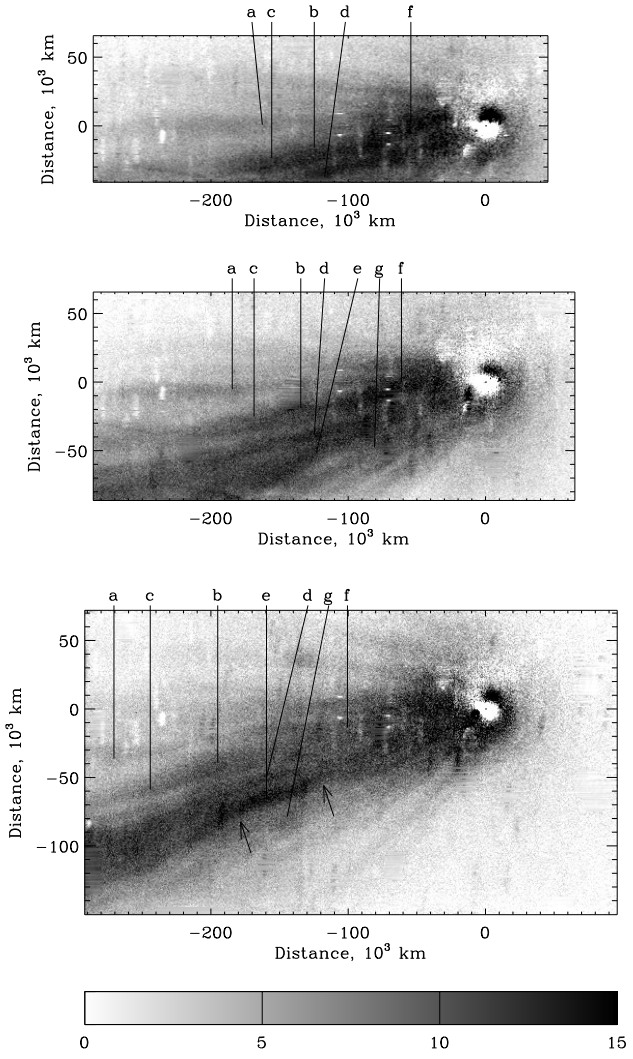

Fig. 4. The continuum subtracted CO^+ images converted to column densities, 10^{10} cm^{-2}. The marked features appear in at least two of the three images. Scales as in Fig. 3.

are not critical, because our further analysis is based on the ion behavior at distances $> 6.6\ 10^4$ km. Moreover, the CO^+ images contain negative values in an area shaped like the spiral jet in the continuum image. No such effect can be seen in the H_2O^+ image. As will be addressed in Sect. 4.2.1, in the CO^+ image the continuum is oversubtracted in this area because the color is redder in the jet than in its surroundings.

Several features appearing in at least two of the three CO^+ images are labeled with lowercase letters. Most of the resolved features are elongated streamers or rays, or condensations which do not exhibit substantial morphological changes during their tailward motion. Only (f) is not very well seen as an isolated feature, particularly in the first image. We have labeled with (f) the cross-point of the prolongations of features (a) and (b-c) to the nucleus. The up-arrows in the lower image point to the positions of two knots, marking the upstream and downstream boundaries of features (d) and (e).

In Fig. 5 we have marked only those structures which have counterparts in the CO^+ images. Below feature (b-c) in the H_2O^+ image there is a narrow streamer. It has not been marked because no counterpart could be found neither in the 2nd, nor in the 3rd CO^+ image. On the other hand, no feature corresponding to condensation (d) in the CO^+ images can be seen in the H_2O^+ image.

4. Discussion

4.1. The ions

4.1.1. Spatial distribution of H_2O^+ and CO^+

The most remarkable feature in our data set is the different spatial distribution of CO^+ and H_2O^+, well seen in Figs. 4 and 5. H_2O^+ possesses a narrower tail and is more concentrated toward the nucleus. CO^+ has a broader tail and a more diffuse distribution. This difference is well seen in the profiles perpendicular to the projected tail axis presented in Fig. 6. Two cuts across the tail are shown at tailward distances 70 and and 170 10^3 km, respectively. The CO^+ column density decreases smoothly with increasing distance from the tail axis. Despite some local variations, resulting from the changing positions of moving features, the overall shape of the CO^+ profiles remains essentially unchanged in the time interval of 1 hour covered by the observations. The H_2O^+ profiles seem to consist of two components,

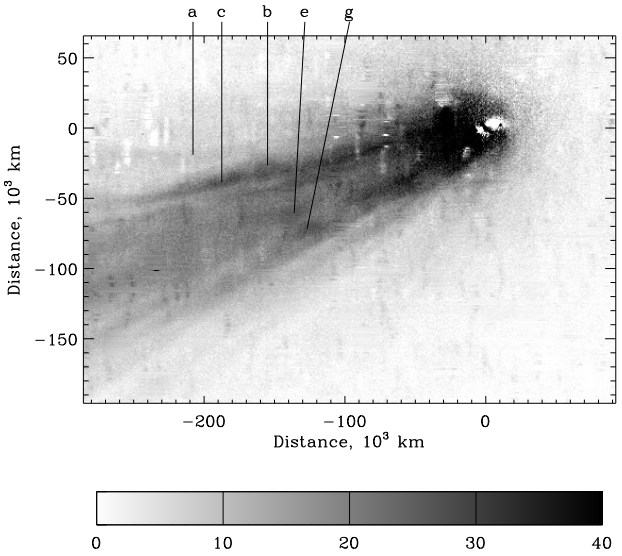

Fig. 5. The continuum subtracted H_2O^+ image converted to column densities, 10^{10} cm^{-2}. Marked are only features having counterparts in the CO^+ images. A ≈17% contribution of the CO^+ (0–2) transition has not been removed. Scales as in Fig. 3.

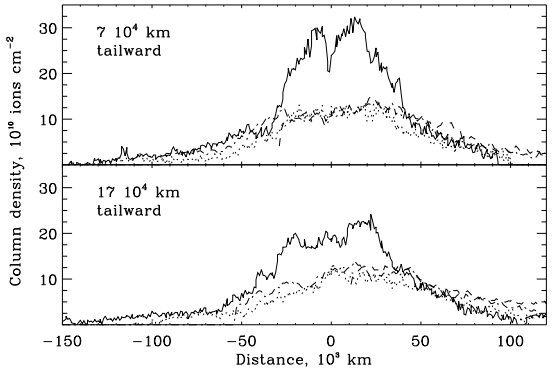

Fig. 6. Cuts perpendicular to the tail axis at distances 7 and 17 10^4 km tailward from the nucleus. The cuts correspond to 5.3 and 13 10^4 km projected distance in Figs. 4 and 5. Solid lines: the water ions. Dashes, dash-dots and dots describe the carbon monoxide profiles in the 1st, 2nd and 3rd CO^+ image, respectively.

a conspicuous concentration close to the tail axis ($< 5\,10^4$ km) and smoothly decreasing wings at larger distances. The central component of the H_2O^+ profiles is reminiscent of the plasma sheet revealed by the ICE measurements in the tail of comet Giacobinni-Zinner (McComas et al. 1987). The CO^+ profiles have similar structure but the concentration around the axis is not so strongly expressed as in the case of H_2O^+, neither near to the nucleus, nor further in the tail. The shape and the strength of the CO^+ profiles change only slightly with increasing tailward distance. At the same time the central component of the H_2O^+ profiles decreases by a factor of about 2 from 7 10^4 to 17 10^4 km in the tail.

The considered profiles reveal the spatial distribution of the ions only locally. The overall picture can be analyzed by means of a histogram analysis. We used the spatially matching areas of our CO^+ and H_2O^+ images to construct the histograms presented in Fig. 7. The right extended wing of the H_2O^+ histogram, belonging to higher column densities, is formed from a relatively small amount of pixels near the nucleus. The CO^+ histogram indicates a rather smooth transition between the pure cometary signal and the lower column density values around the histogram peak, where the cometary contribution is mixed with background signal.

The difference between the spatial distribution of CO^+ and H_2O^+ supports the magneto-hydrodynamic simulations by Wegmann et al. (1987). These authors have modeled the physics and chemistry in the coma of P/Halley in great detail and have evaluated column densities of different ions for comparison with ground-based observations. The CO^+ and H_2O^+ maps presented by Wegmann et al. (1987) confirm what we observe in comet P/ST, namely that the H_2O^+ distribution is more concentrated toward the nucleus and around the tail axis.

The different spatial extent of CO^+ and H_2O^+ can be understood by comparing the channels for their production and the scale lengths of their most probable parents, CO and H_2O. Photoionization is the main process responsible for the production of both ions. During intermediate solar activity conditions, the photoionization and photodissociation rates of CO are 3.8 10^{-7} s^{-1} and 2.8 10^{-7} s^{-1}, respectively (Schmidt et al. 1988). Even if the charge exchange mechanism is included, except of extremely enhanced solar wind flux, the scale length of CO will be several hundred thousand kilometers (Fernandez & Jockers 1983). On the contrary, neutral water has a very high photodissociation rate, 1.03 10^{-5} s^{-1} (Schmidt et al. 1988), which shortens its scalelength to less than 10^5 km. Cochran & Schleicher (1993) argue in favor of even shorter lifetime of cometary H_2O. Hence, the difference between the CO^+ and H_2O^+ spatial distribution is related to the different extent of their sources, the neutral clouds of their parent molecules. Consideration of the photodissociative ionization of CO_2 as an alternative or additional mechanism for CO^+ production would not change this situation because of the low rate coefficient of this reaction. Possible existence of an extended source, as it has been found in Halley's comet (Eberhardt et al. 1987), would further increase the region where CO^+ can be born.

4.1.2. Tail structures

Comet P/ST had a very complex structured plasma tail. The most prominent features, labeled as (a), (b-c), (d) , and (e) in the three CO^+ images, shown in Fig. 4, can be considered as markers along four well separated streamers.

The appearance of structures in the H_2O^+ image differs from the structures in the CO^+ images. In the H_2O^+ image the two outer elongated condensations (rays) along features (b-c) and (g) dominate the surrounding plasma. In the CO^+ images the condensations are more uniformly distributed across the tail and can be seen farther from the tail axis than in the H_2O^+ image. Feature (b-c) appears narrower in the H_2O^+ image than

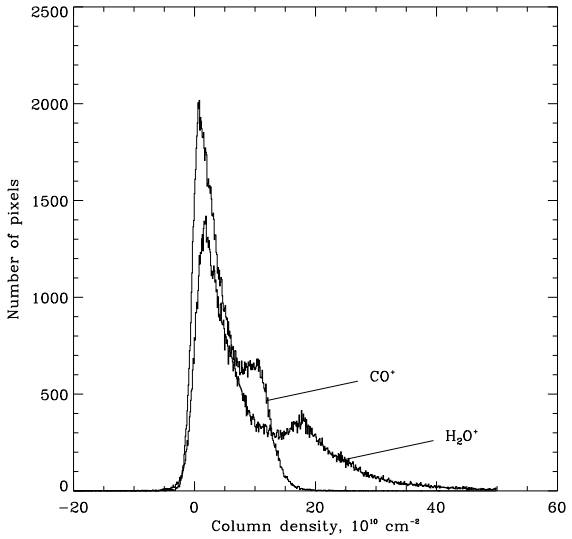

Fig. 7. Histograms of the final CO^+ and H_2O^+ images. The narrower CO^+ histogram is an illustration for the flatter distribution of CO^+. The feature in the right wing of the H_2O^+ histogram indicates the existence of higher column density concentrated in a relatively small zone around the nucleus.

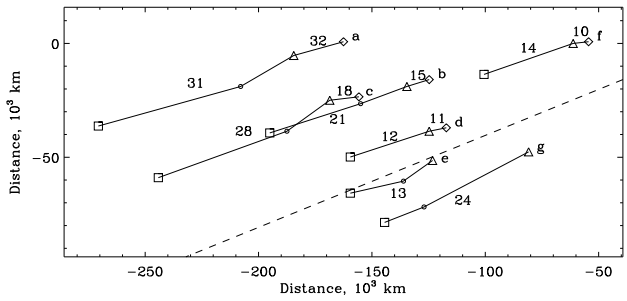

Fig. 8. The location of tail structures in the plane of sky derived from tracing the condensations in the plasma images. The dashed line shows the antisolar vector. The motion of the structures goes from right to left along the full lines (see text). The circles denote the H_2O^+ image, the other symbols the three CO^+images. The numbers indicate the derived sky plane velocities spv.

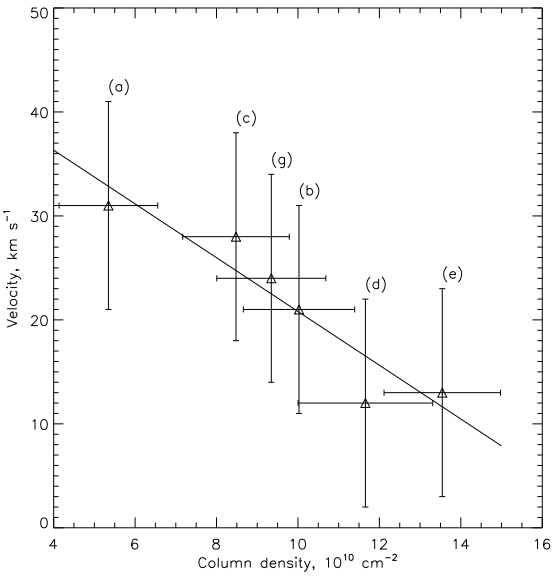

Fig. 9. Relation between sky plane velocities spv of the tail structures and their mean column densities. The features are marked as in Fig. 4. The full line is a linear fit through the data.

in the CO^+ images. Although the H_2O^+ image was obtained 21 minutes after the 2nd CO^+ image and 29 minutes before the 3rd one, more similarities can be found between both CO^+ images than between each of them and the H_2O^+ image. This is an indication that the observed dissimilarities between the structures in the CO^+ and H_2O^+ images might be present not only temporarily.

The traces of the features marked in Figs. 4 and 5 are presented in Fig. 8. Diamonds, triangles, and squares stand for the positions of condensations in the first, second and third CO^+ image. respectively. The circles represent the location of the features in the H_2O^+ image. The numbers at the trajectories are the velocities projected in the sky plane (henceforth sky plane velocities spv) in km s^{-1}). They are calculated by using only the three CO^+ images. The dashed line represents the projection of the comet's prolonged radius-vector. The velocity increases with increasing distance from the nucleus. Moreover, in agreement with *in situ* measurements (Siscoe et al. 1986) and with MHD modeling (Rauer et al. 1995 and references therein), the velocity is low near to the tail axis and increases to greater lateral distances.

The velocity of the structures and their mean column densities are anticorrelated, as it can be seen in Fig. 9. The error bars of the velocities are derived from the tracing process. The errors of the column densities are $1\,\sigma$ values in boxes of size 11×11 pixels around each condensation in the third CO^+ image. The full line is a linear fit through the data. The existence of such an anticorrelation was pointed out by Jockers (1985) but no quantitative regression could be derived at that time.

Rauer & Jockers (1993) have shown that the apparent motion of structures in the ion tail of a comet is a manifestation of the bulk plasma flow, rather than a wave phenomenon. In the case of comet P/ST we can check this and in this way gain confidence in our velocity measurements by comparing our velocity field with Doppler measurements of other authors. If we assume that the plasma tail orientation is exactly along the antisolar direction, then the line of sight velocities (hereafter lsv), obtained by Doppler measurements, and the velocities in the sky plane (spv), obtained by tracing of plasma structures, are related by the expression $spv = \tan(\phi) \times lsv$, where ϕ is the phase angle. In our case, $\phi \approx 49°$ and we should expect apparent velocities in the sky plane about 15% greater than the measured line of sight velocities.

Brown et al. (1993) and Spinrad et al. (1994) (both papers referred to as BSJ93 hereafter) provide radial velocity measurements of H_2O^+ along the tail of comet P/ST out to a distance of 4 10^5 km. Unfortunately, in their set of observations there

are no measurements on Nov 25, 1992. Therefore we are forced to look if a reasonable information can be extracted from the values obtained on neighboring days. The lsv measurements by BSJ93 do not show any significant temporal variations up to 2 10^5 km in the tail in the time interval Nov 23 - Dec 1, 1992. So, with some reservations, we could consider a mean value of these measurements as representative for Nov 25, too. Averaging the four measurements from this time interval we obtained a mean value of the lsv = 13 $\pm$ 3 km s^{-1} at 1.5 10^5 km projected distance in the tail.

As the long slit in the spectroscopic observations of BSJ93 was oriented along the tail, only velocities of those structures should be used in the comparison, which are near to the tail axis in our observations . These are (d), (e), and (g) in Fig. 8. The apparent velocities of these condensations in the sky plane are in agreement with the mean value of Doppler measurements, despite of the lsv values being derived from H_2O^+ and the spv velocities from CO^+. This is an indication that the moving structures, mostly observed in the light of CO^+, allow to derive valid velocities for the CO^+ as well as for the H_2O^+ ions within the uncertainty of our measurements of $\pm$10 km s^{-1}. These velocities can be used to calculate the ion flux of both types of ions in the plasma tail of comet P/ST.

4.1.3. The ion flux

Once a cometary ion is born in the source region it is picked up by the solar wind and accelerated tailwards. No matter where it has appeared, inevitably it leaves the source region tailwards. If at a certain tail cross-section the density of the ions and their tailward velocities are known it is possible to calculate the ion flux at this cross-section. In what follows we will use a coordinate system originating at the nucleus and with x, y, and z-axis directed, respectively, along the projection of the antisolar direction, perpendicular to x in the sky plane, and along the line of sight. Then the total ion flux through a plane crossing the tail at a distance x' from the nucleus, is given by:

$$F(x') = \int_{-\infty}^{\infty} v_x(x', y)\, N(x', y) d\, y \qquad (4)$$

Here $N(x')$ denotes the observed column densities, $v_x(x')$ are the tailward velocities, projected on to the sky plane, and the integration is performed perpendicular to the projected tail axis. At first glance we know all quantities needed to calculate the ion flux, namely the measured column densities and the velocities obtained from the tracing of plasma structures. The problem is that we can associate velocities only with a very limited number of selected, more dense structures in the ion tail, but we do not know the velocities in the ambient plasma. What we need is a velocity profile across the tail. BSJ93 have measured velocities perpendicular to the tail, but unfortunately only a week later than our observations, on Dec 2, 1992. Another problem in the straightforward use of these observations is that they finish at a lateral distance from the tail axis of 4 10^4 km and 6 10^4 km, respectively. These distances are in agreement with the extent

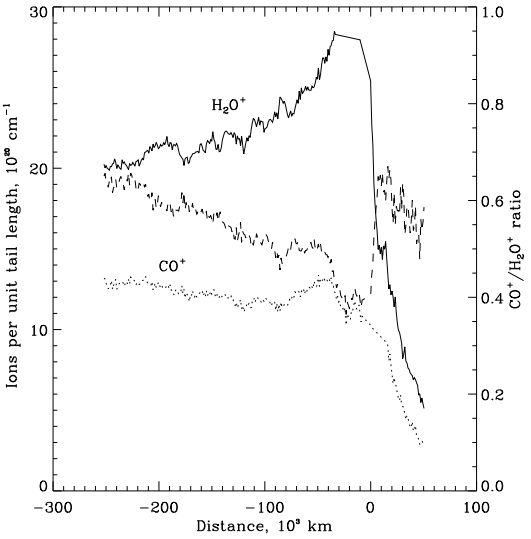

Fig. 10. Ions per unit tail length and the CO^+/H_2O^+ ratio plotted versus deprojected distance from the nucleus.

of the central concentration in the profiles, discussed in the previous subsection, but we observe non-zero column densities at greater distances from the tail axis, too. What to multiply these column densities with?

Taking into account that it is impossible to associate a velocity measurement with each measured column density, we will estimate the ion flux in the tail of comet P/ST using mean values. If we denote the mean flow speed in a cross-section perpendicular to the tail axis as $\bar{v}_x(x')$ (Bonev & Jockers 1994), the total ion flux is given by:

$$F(x') = \bar{v}_x(x') \times \eta(x'), \qquad (5)$$

where $\eta(x') = \int N(x', y) d\, y$ is the mean number of ions per unit projected tail length.

Integrating the column densities across the tail in our CO^+ and H_2O^+ images, we found the spatial distributions of $\eta(CO^+)$ and $\eta(H_2O^+)$, presented in Fig. 10 together with their ratio.

The profiles of the ions per unit tail length are significantly different for both ions. As in comet Austin 1990 V (Bonev & Jockers 1994) $\eta(H_2O^+)$ decreases at distances $> 5\ 10^4$ km. This trend is not seen in the case of CO^+. Most probably this again is caused by the different scale lengths of the parents of both ions. Beyond 5 10^4 km the amount of H_2O^+ ions added to the plasma flow decreases strongly. As H_2O^+ is rather stable outside the inner coma it can be assumed that the H_2O^+ flux remains constant outside of the source region. At the same time the ions are accelerated tailwards. Under these conditions, according to Eq. 5, the number of ions per unit tail length decreases. For CO^+, the nearly constant η-value might be a consequence of the greater scale length of their parents, which feed the plasma flow even far from the nucleus with new ions, enough to compensate for the dilution caused by the acceleration.

The structures in our images, except (f), can be considered as defining a cross-section perpendicular to the axis at about

1.5 10^5 km in the tail of comet P/ST (see Fig. 8). Using the velocities, weighted by the column density of each structure, we found a mean sky plane velocity spv of 20 km s^{-1}. This value, associated with the whole cross-section of the tail at 1.5 10^5 km, is greater than the local velocities measured on the axis at the same distance (structure (e)), which is in agreement with MHD models of the plasma flow in a comet (Wegmann, private communication). With this mean velocity and with the η values taken at the same distance we derived fluxes of $4.2 \pm 1.4\ 10^{27}$ s^{-1} and $2.4 \pm 0.8\ 10^{27}$ s^{-1} for the H_2O^+ and CO^+ ions, respectively. The projected distance of 1.5 10^5 km corresponds to a real, deprojected distance from the nucleus of 2 10^5 km. The largest contribution to the error comes from the velocity determination. The error of the scale factor is of minor importance, as we are concerned with the large projected distance of 1.5 10^5 km downstream of the nucleus. In addition we recall that for the H_2O^+ lines in our filter passband we have somewhat arbitrarily assumed half the g-factor of the 0-8-0 transition.

It is interesting to compare the obtained water ion flux with measurements of the water production rate during this time. On Oct. 15, 1992 Colom et al. (1992) observed P/ST with the Nancay Radio Telescope and estimated an OH production rate of 8 10^{28} s^{-1}. Water production rates can be derived from the OH radio lines following the model of Bockelée-Morvan et al. (1990), who argue that Q(H_2O) = 1.1 Q(OH). Taking into account that in the period from Oct. 15 to Nov. 25 the heliocentric distance of the comet r changed from 1.35 to 1.00 AU, and that the gas production dependence is steeper than r^{-2}, we derive a lower limit of 1.6 10^{29} s^{-1} for the water production on Nov 25. Tozzi et al. (1994) have inferred a water production rate of $\approx 2 \times 10^{29}$ s^{-1} from IUE observations on November 16. Later, at the beginning of December 1992, Bockelée-Morvan et al. (1994) found that the OH production rate was several 10^{29} s^{-1}. Fink & Hicks (1996) measured the emission flux of the [OI] 6300 Å line in P/ST and, thereby, derived a water production rate of 9.5 10^{29} s^{-1} and 8.8 10^{29} s^{-1} on Nov 24 and Nov 26 1992, respectively.

The values of Fink & Hicks are rather high. Nevertheless we adopt them for our discussion, because they were obtained closest to our date of observations. Then, when comet P/ST was at 1 AU heliocentric distance, the ratio $H_2O/H_2O^+ \approx 220$. The obtained ratio of neutral water to water ions is greater than in the MHD model of P/Halley by Wegmann et al. (1987), the model with the most detailed treatment of the physical conditions and chemical reactions in a cometary coma. In this model the production rate of water is 5.5 10^{29} s^{-1} (total gas production rate of 6.9 10^{29} mol s^{-1}, 80% of which being water). Integrating the H_2O^+ column densities (Fig. 7 in Wegmann et al. 1987) perpendicular to tail axis at 10^5 km tailward from the nucleus we found $\eta \approx 1.3\ 10^{21}$ cm^{-1}. Using the velocity maps of Wegmann et al. (1987) supplemented by private communication from these authors we obtain the mean velocity $\bar{v}_x(x' = 10^5\text{km}) = 40$ km s^{-1}. This gives a flux of $H_2O^+ = 5.2\ 10^{27}$ s^{-1} and a ratio $H_2O/H_2O^+ \approx 105$.

If only photodissociation and photoionization of water are considered, about 3% of the neutral water should end up as water ions. This is about 3 times more than the value found by Wegmann et al. (1987). In the inner coma, where the neutral water density is sufficiently high, water ions are lost by the reaction

$H_2O^+ + H_2O \rightarrow H_3O^+ + OH$

Another destructive channel is the dissociative recombination. Schmidt et al. (1988) pointed out that as soon as the water ion becomes dominant the reaction

$H_2O^+ + e \rightarrow OH + H$

dominates the other recombination processes. Most probably, these two mechanisms are responsible for the destruction of about two of three created H_2O^+ ions, explaining thus why in a detailed model about 1% of the neutral water ends up as water ions. Water ion destruction is important only in the inner coma, i. e. our previous discussion on the total ion fluxes in the plasma tail remains valid.

Our measured H_2O/H_2O^+ ratio of ≥ 200 is greater than both the value of ≈ 33 derived from the simple comparison of photodissociation and photoionization of water and the value 105 of the MHD model of Wegmann et al. (1987). It is possible that part of the ions remained undetected in our measurements, namely the ions at greater distances from the tail axis, where the signal/noise ratio is insufficient. They can give a considerable contribution to the ion flux, because their velocities are high. The problem of nondetection of fast moving ions has been discussed in Jockers (1991), Rauer and Jockers (1993), and Bonev & Jockers (1994). When the comparison of measured fluxes has been made with values based on the simple photodissociation – photoionization model, the amount of the nondetected ions has been overestimated. Our analysis shows that most probably there remains an underestimation of the H_2O^+ ion flux but this effect is not as strong as previously believed. The comparison of the H_2O^+ flux with water production values derived from extrapolated OH measurements yields a lower H_2O/H_2O^+ ratio, in better agreement with Wegmann et al. (1987).

It should be noted that, for several reasons, in the calculation of the CO^+ flux a greater underestimation has to be expected as compared to the H_2O^+ flux. First, our measurement of the ions per unit tail length can not account for ions at larger lateral distances from the tail axis, because of observational restrictions (detector sensitivity and limited field of view). Second, $\bar{v}_x(x')$ is expected to be greater for CO^+ than for H_2O^+, because a larger contribution of CO^+ ions at greater distances from the tail axis. And third, the deprojected distance of 2 10^5 km is still in the source region of CO^+ ions.

4.1.4. The CO^+ to H_2O^+ ratio

From the observational point of view different kinds of CO^+/H_2O^+ ratios can be defined, the ratio of column densities, ratio of the ions in tail cross-sections, or the ratio of the total ion content. Fig. 6 shows that the ratio of the column densities increases from a mean value of about 0.5 on the axis to ≈ 1 at lateral distances > 6 - $7\ 10^4$ km. The ratio between the ions per unit tail length, presented in Fig. 10, increases from about 0.52 at 1 10^5 km deprojected distance to more than 0.6 at $> 2\ 10^5$

km. Because of contamination close to the nucleus we cannot quote a value for the total ion content.

Most suitable for comparison with other observations is the column density ratio measured on the tail axis. Lutz et al. (1993) have measured a mean value $CO^+/H_2O^+ \approx 0.3$ between 1 10^4 and 3 10^5 km in the plasma tail of P/Halley. In comet P/ST we find a value of 0.39 close to the axis at a tailward distance of 7 10^4 km. At the distance of 17 10^4 $CO^+/H_2O^+ = 0.58$. The errors are 7% (9%) at 7 10^4 km and 4% (6%) at 17 10^4 km. The errors in the brackets include the photometric error in the ratio of the two wavelengths. Apart from photometry the scale factor (Eq. 1) contributes the largest error to this estimate. As the relative contribution of the ion emission to the on-line image increases along the tail, the error decreases with increasing distance into the tail. This higher value of the CO^+/H_2O^+ ratio might be an indication that in P/ST the relative abundance of CO and CO_2 with respect to H_2O is greater than in P/Halley. When P/Halley was observed by Lutz et al. (1993), it was at a heliocentric distance of about 1.3 AU, larger than the distance of 1.0 AU of P/ST during our observations, but sufficiently close to the Sun that water readily sublimes. Therefore, as was shown by A'Hearn et al. (1995), the ratios between gaseous species measured at 1.3 AU can be used at 1.0 AU with little error.

Additional evidence for a greater relative abundance of CO^+ parents with respect to H_2O in P/ST than in P/Halley comes from the comparison with model results. The column densities, presented in the model of P/Halley by Wegmann et al. (1987), yield a value of about 0.25 for the CO^+/H_2O^+ ratio near to the axis, at a tailward distance 1 10^5 km. Fink & Hicks (1996) have shown that P/ST has a higher gas production rate than P/Halley at the same heliocentric distance. According to the scaling laws in MHD (Wegmann 1995), when all other conditions are unchanged, the model spatial scale expands for comets with higher production rates. At distances $> 10^5$ km we measured $CO^+/H_2O^+ > 0.5$, with a tendency of increasing further tailwards. Thus the CO^+/H_2O^+ column density ratio in P/ST is significantly greater than the one derived by MHD modeling of P/Halley. This supports our statement that the abundance of CO-bearing molecules relative to H_2O is slightly increased in P/ST in comparison to P/Halley. It should be noted, however, that this discussion depends on the proper selection of the fluorescence efficiency factor for the H_2O^+ ions in our filter, which was rather arbitrarily assumed to be half of the total 0-8-0 transition.

Having found a satisfactory agreement in the comparison of our data with both other observations and model results, it is tempting to check if a simplified consideration of the same subject would give similar results. CO^+ is produced mainly by photoionization of carbon monoxide and, near to the nucleus, by photodissociative ionization of carbon dioxide. However, theoretical modeling by Huebner and Giguere (1980) shows that only about 10% of the total CO^+ production comes from CO_2. Thus, in a first approximation, the observed CO^+ densities can be considered as reflecting mainly the CO abundance in a comet.

According to Huebner (1985), the branching ratio of the reaction

$$CO + h\nu \rightarrow CO^+ + e^-$$

is about 0.5. Several processes are contributing to the production of H_2O^+ but the dominant one is the photoionization of neutral water:

$$H_2O + h\nu \rightarrow H_2O^+ + e^-$$

with a branching ratio of about 0.03. The consideration of only these two channels of ion production yields following relation between the parent species and their daughters:

$$CO/H_2O = 0.06 \times CO^+/H_2O^+$$

With $CO^+/H_2O^+ = 0.3$, the mean value measured by Lutz et al.(1993) in the tail of P/Halley, we obtain a CO/H_2O ratio of 0.02, much less than the value derived from *in situ* measurements of P/Halley (Eberhardt et al. 1987). This contradiction shows how the result would be biased in the case of a simplified treatment of measured CO^+ and H_2O^+ ion densities. At the same time, the agreement with the detailed MHD model by Wegmann et al. (1987) illustrates the importance of accounting for all known chemical and physical processes in the inner coma of a comet. It also indicates that within the observational uncertainties the Wegmann et al. model is complete.

4.2. The dust

4.2.1. The dust color

The scaling factors, obtained in the process of continuum subtraction, allow to derive the color of the dust in the spectral range of our observations. A good useful measure of the continuum color is the normalized gradient of the reflectivity, $S'(\lambda_1, \lambda_2)$ (A'Hearn et al. 1984; Jewitt 1991):

$$S'(\lambda_1, \lambda_2) = \frac{1}{\bar{R}} \frac{\partial R}{\partial \lambda} = \frac{R(\lambda_2)/R(\lambda_1) - 1}{R(\lambda_2)/R(\lambda_1) + 1} \frac{2}{\Delta\lambda} \quad (6)$$

where R is the reflectivity at given wavelength, λ, and $\bar{R}$ is the mean reflectivity within a wavelength range $\lambda_1 \leq \lambda \leq \lambda_2$. In our case the ratio between the reflectivities at both considered wavelengths is equivalent to the ratio between expected response of the instrumentation to solar continuum radiation and the empirically obtained continuum scaling factor. Applying the definition of the normalized gradient of the reflectivity (6) to the data in Table 3, we find the following colors for the dust in comet P/ST:

$$\begin{aligned} S'(4260, 6420) &= 0.05 \pm 0.01 \\ S'(4260, 6420)_j &= 0.11 \pm 0.01 \\ S'(6200, 6420) &< 0.01 \pm 0.01 \\ S'(6200, 6420)_j &< 0.01 \pm 0.01 \end{aligned} \quad (7)$$

The reflectivity gradients in (7) are reduced to $\Delta\lambda = 1000$ Å. The subscript j stays for the cases in which a good removal of the jet was achieved, i.e. these are the colors of the dust particles residing in the jet. Positive values correspond to reddening of the dust. Negative values would indicate that the dust is bluer than the solar spectrum. The dust in comet P/ST is redder in the spectral region between 4260 Å and 6420 Å, and this reddening

is stronger for the particles residing in the jet. A stronger reddening in a jet as compared to the diffuse dust coma was found by Hoban et al. (1989) in P/Halley. In a recent paper Kolokolova et al. (1996) show that the dust color is mainly determined by the grain size distribution. Hence, the stronger reddening observed in cometary dust jets might indicate that the spatially isolated eruptive event on the nucleus causing the jet produces relatively more grains with greater sizes than the process of continuous release of dust particles from the cometary surface. More detailed conclusions can possibly be drawn about the dust properties in comet P/ST if our results are considered in combination with polarization and infrared measurements. Recently, Eaton et al. (1995) found that the polarization is up to 4% higher in the jet than in the surrounding coma in this comet. Goldberg and Brosh (1995) argue that the polarization in the jet region is higher than values typical for 'dusty' comets.

The accuracy of our measurements does not allow to be confident about the color in the spectral region around 6300 Å.

4.2.2. Radial profiles and dust production

In the case of a steady state radial outflow from a central source one would observe a surface brightness decrease of the dust coma $\propto \rho^{-1}$, where ρ is the projected distance from the source. In comet P/ST, which is well known for its activity, to a large extent the dust coma and tail are replenished by a number of spatially localized outbursts, rather then by steady release of dust particles from the whole nucleus. Our single continuum image, presented in Fig. 3, reveals a highly inhomogeneous dust distribution in the inner coma. A detailed description of this very complex coma would require elaborate modeling, accounting for each structure individually, e.g. in a way as it has been done by Sekanina (1981). We will concentrate here only on some more general features of the dust distribution.

The radial profiles along the projected sunward and antisunward directions are well described by a power law with exponents of -1.73 and -1.25, respectively. In deriving both values we excluded the innermost part of the image ($<$ 7 - 8 arcsec) which is blurred by a systematic tracking error. Outside this region the obtained exponents are constant throughout the whole field of view.

For the study of the mean dust distribution we have averaged the continuum image azimuthally around the nucleus. The result is shown in the upper panel of Fig. 11. The nearly constant region in the innermost part is an artifact caused by the above mentioned tracking error. The logarithmic gradient of the linear section between 5 10^3 and 4 10^4 km is -1.4. The faster decrease of the surface brightness might be caused by radiation pressure acceleration of the dust particles. Another explanation could be a gradual fading of the grains in their outward motion. Most probably both effects contribute to the fact that the brightness decreases faster than expected in the case of simple radial outflow with constant velocity. A transition of the logarithmic gradient from -1.4 to -1.9 is seen at about 4 10^4 km. This is approximately the distance to which the spiral jet extends. We could speculate that the particles in the jet are not so strongly influenced by the radiation pressure as the ambient dust. Therefore their contribution to the brightness reduces the slope in the inner part of the coma. Such an explanation is in agreement with our previous argument that the grains in the jet should have larger sizes.

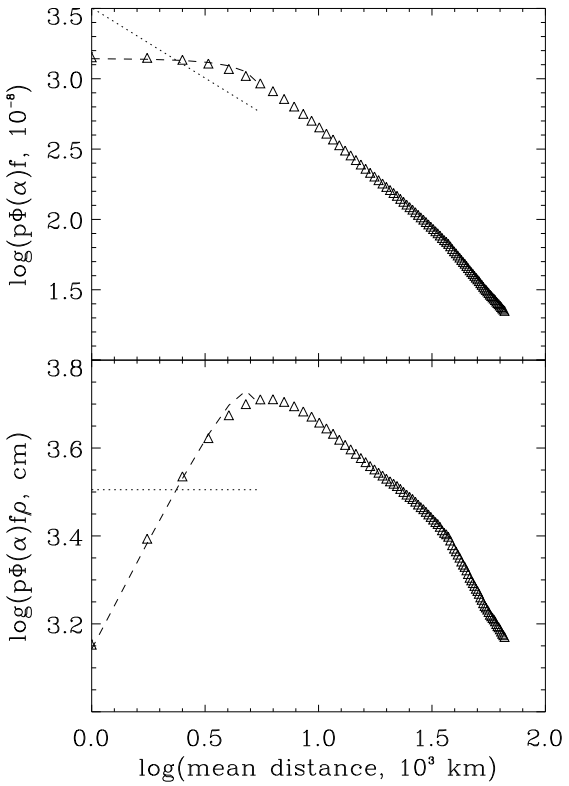

Fig. 11. Upper panel: The product between geometric albedo, phase function and filling factor as a function of projected distance to the nucleus ρ. Lower panel: The product between geometric albedo, phase function, filling factor, and projected distance.

As a measure of the dust production, A'Hearn et al. (1984) have introduced the quantity $Af\rho$, the product of albedo, filling factor of grains within the field of view, and the linear radius of the field of view at the comet. Based on the assumption of a simple radial outflow this quantity is independent of the field of view, giving thus the opportunity to compare measurements obtained under different geometrical conditions. In a similar way we have calculated the quantity $p\Phi(\alpha)f\rho$, presented in the lower panel of Fig. 11. Recall that the geometric albedo, p, used in our calculation is one quarter of the Bond albedo, A, used by A'Hearn et al. (1984). Moreover, our local filling factor is one half of the aperture integrated value of A'Hearn et al.

(1984)[1]. Thus, in order to compare our $p\Phi(\alpha)f\rho$ quantity with $Af\rho$ values, the latter should be divided by 8.

The outward increase of $p\Phi(\alpha)f\rho$ near to the nucleus reflects simply the blurring of the inner coma by incorrect guiding. If in reality there was a constant section of $p\Phi(\alpha)f\rho$ in this inner most region, it should appear at a level below the value of the artificial maximum. In order to check if the averaged radial profile in the inner most region of the dust coma can be described by an ρ^{-1} brightness distribution we modeled numerically the smearing imposed on our continuum image. The result of this simulation is shown in both panels of Fig. 11. The dotted line represents the unsmeared ρ^{-1} model and the dashed line is obtained by smearing this model in the same way as it happened during the observations. The good fit of this rather simple model to the measured data allows to deduce a value of $p\Phi(\alpha)f\rho \approx 3200 \pm 600$ cm for P/ST. The quoted error derives from the known amount of incorrect guiding and the photometric error.

Osip et al. (1992) provide a value of $log(Af\rho) = 4.28$ for comet Halley during the Giotto encounter. At this time the phase angle of P/Halley was 65° for the ground-based observer. We observed P/ST at a phase angle 49°. Both values are in a range where the phase function of cometary dust shows little variation (Ney 1982), thus no correction is needed for the phase function. Dividing the value of Osip et al. (1992) by 8 we obtain $p\Phi(\alpha)f\rho) \approx 2400$ cm for P/Halley during the Giotto encounter. The extrapolation of this value by application of a r_H^{-2} heliocentric dependence of the dust production, yields a value $p\Phi(\alpha)f\rho) \approx 2000$ cm for P/Halley at 1 AU, the distance at which we observed P/ST. Osip et al. (1992) claim that the r_h^{-2} dependence is typical for the dust of most comets in their data base. Thus, if the physical characteristics, chemical composition, and the outflow speeds of the dust particles in both comets were the same, comet P/ST had about 1.6 times greater dust production than P/Halley at the same heliocentric distance. As the gas productions of both comets differ by almost the same factor the dust to gas ratio should be comparable in comets P/Halley and P/ST.

5. Conclusions

We have analyzed narrow-band CCD-images revealing the spatial distribution of H_2O^+, CO^+, and dust in comet P/Swft-Tuttle. At a distance of 2 10^5 km tailward from the nucleus the number of ions per unit tail length was 2.1 10^{21} cm^{-1} water ions and 1.2 10^{21} cm^{-1} CO^+ ions.

The plasma tail of P/Swift-Tuttle was highly structured. We found indications that some of the structures seen in the CO^+ images do not have counterparts in the H_2O^+ image and vice versa. Do different ions form their own structures in a cometary plasma tail? The study of this subject requires simultaneous observations of both ions.

Using velocity measurements, obtained by tracing the plasma structures in our images, we calculated a mean flux of water ions in the tail of comet P/Swift-Tuttle of about 4.2 10^{27} s^{-1}. The comparison of this value with estimations for the neutral water production yields good consistency with the MHD models of Wegmann et al. (1987).

The spatial extent of the CO^+ images is greater than that of H_2O^+ which is indicative for a larger source region for the CO^+ ions as compared to H_2O^+, in accordance with MHD models. The results agree within observational errors with the MHD model of Wegmann et al. (1987), which includes detailed gas phase chemistry.

The CO^+/H_2O^+ ratio increases from 0.52 at a tailward distance of 10^5 km to 0.58 at 2 10^5 km. This value is higher than the value observed in comet P/Halley. This might be considered as an indication that the abundance of CO-bearing molecules in the surface layers of the nucleus of comet P/Swift-Tuttle is increased as compared to comet Halley.

The analysis of the continuum image has shown that in the spectral range 426 - 642 nm the particles in a jet, observed near to the nucleus, and in the ambient dust have a different reddening, 11% and 5% per 1000 Å, respectively.

It was found that the comet Swift-Tuttle's dust production has been about 1.6 times greater than comet Halley's at the same heliocentric distance and that the dust to gas ratio in both comets is comparable.

Acknowledgements. We would like to thank S. Zhekov, who kindly provided part of his observing time on Nov 25, 1992 and assisted during the observations. No observations would have been obtained without the cooperation of the staff of BNAO, Rozhen. The authors thank R. Wegmann for sending model velocities and for numerous discussions concerning them. We are grateful to H. Spinrad and coworkers for additional information on their velocity measurements. We also thank M. A'Hearn and U. Fink for sending papers prior to publication. T. B. acknowledges the hospitality of the Max-Planck-Gesellschaft, which allowed him to work several weeks at the MPAe, where this study has been started. This work was supported in part by the Bulgarian National Science Foundation under contract F-482 with the Ministry of Science and Education. Comments by an anonymous referee led to a significant improvement of the paper.

References

A'Hearn, M. F., Millis, R. L., Schleicher, D. G., Osip, D. J., Birch, P. V. 1995, Icarus, 118, 223

A'Hearn, M. F., Schleicher, D. G., Feldmann, P. D., Millis, R. L., Thompson, D. T. 1984, AJ, 89(4), 579

A'Hearn, M. F., Festou, M. C. 1990, in Physics and Chemistry of Comets, ed. Huebner, W. F., Springer-Verlag Berlin Heidelberg

Bockelée-Morvan, Crovisier, J., Gérard, E. 1990, A&A, 238, 382

Bockelée-Morvan, D., Bourgois, G., Colom, P. et al., 1994, Planet. Space Sci., 42(2), 193

[1] A'Hearn et al. use a total filling factor, $f_{TOT} = N\sigma/(\pi\rho^2)$, where N is the total number of scattering particles within a diaphragm with radius ρ, and σ is the mean cross-section of the grains. With a constant outflow velocity, v, the expression can be written as $f_{TOT} = \dot{N}\tau\sigma/(\pi\rho^2) = \dot{N}\sigma/(\pi\rho v)$, where $\dot{N}$ is the production rate of dust particles and τ is the age of the oldest particles in the field of view, i.e. the particles which are just reaching the edge of the diaphragm. Here, at a distance ρ from its center, the local filling factor used in our calculation is $f = \dot{N}\sigma/(2\pi\rho v)$, i.e. $f = f_{TOT}/2$. This factor of 2 was erroneously not taken into account by Jockers et al. (1993).

Boehnhardt, H., Birkle, K. 1994, A&AS, 107, 101
Bonev, T., Jockers, K. 1994, Icarus, 107, 335
Brown, M. E., Johns, C.M., Spinrad, H. 1993, GRL, 20, 1003
Cochran, A.L., Schleicher, D.G. 1993, Icarus, 105, 235
Colom, P., Bockelée-Morvan, D., Bourgois, G. et al., 1992, IAU Circ., No. 5643
Cowan, J. J., A'Hearn, M. F. 1979, Moon and Planets, 21, 155
Eaton, N., Scarrott, S. M., Draper, P. W. 1995, MNRAS, 273, L59
Eberhardt, P., Krankowsky, D., Schulte, W. et al., 1987, A&A 187, 481
Fernández, J. A., Jockers, K. 1983, Rep. Prog. Phys., 46, 665
Fink, U., Hicks, M. D. 1996, ApJ, 459, 729
Goldberg, Y., Brosh, N. 1995, MNRAS, 273, 431
Green, D. W. E. 1993, Intern. Comet Quart., 15(4), 182
Hoban, S., A'Hearn, M. F., Birch, P.V. et al., 1989, Icarus, 79, 145
Huebner, W. F., Giguere, P. T. 1980, ApJ, 238, 753
Huebner, W. 1985, in The Photochemistry of Atmospheres, ed. R. Levine, New York Academic Press, 437
Jewitt, D. 1991, in Comets in the Post-Halley Era, eds. R. L. Newburn, Jr. et al., Vol.1, 19
Jockers, K. 1985, A&A Suppl. Ser., 62, 791
Jockers, K. 1991, in Cometary Plasma Processes, Ed. Johnstone, A.D., 139
Jockers, K. 1992, Astronomische Gesellschaft, Abstract Series, 7, 184
Jockers, K. 1995, Astronomische Gesellschaft, Abstract Series, 11, 34
Jockers, K., Kiselev, N. N., Boehnhardt, H., Thomas, N. 1993, A&A, 268, L9
Jorda L., Colas, F, Lecacheux, J. 1994, Planet. Space Sci., 42, 699
Karttunen, H., Kröger, P., Oja, H., Donner K. J. (eds.) 1987, Fundamental Astronomy, Springer, Berlin
Kolokolova, L., Jockers, K., Chernova, G., Kiselev, N. 1996, Icarus, in press
Kurucz, R. 1985, Solar flux Atlas, Cambridge, Harvard University
Lutz, B.L., 1987, ApJ, 315, L147
Lutz, B.L., Womack, M., Wagner, R. M. 1993, ApJ, 407, 402
Magnani L., A'Hearn M.F. 1986, ApJ, 302, 477
Marsden, 1992, IAU Circ., 5636
McComas, D. J., Gosling, J. T., Bame, S. J. 1987, JGR , 92, 1139
Ney, E. P. 1982, in Comets, ed. Wilkening, L. L., University of Arizona Press, Tucson, 323
Osip, D. J., Schleicher, D. G., Millis, R. L., 1992, Icarus, 98, 115
Rauer, H., Jockers, K. 1993, Icarus, 102, 117
Rauer, H., Wegmann, R., Schmidt, H. U., Jockers, K. 1995, A&A, 295, 529
Sanwal, B. B., Rautela, B. S., Singh, M., Srivastava, J. B. 1994, Earth, Moon, and Planets, 64, 139
Schmidt, H. U., Wegmann, R., Huebner, W. F., Boice, D. C. 1988, Comp. Phys. Comm., 49, 17
Sekanina, Z. 1981, AJ, 86, 1741
Siscoe, G. L., Slavin, J. A., Smith, E. J., Tsurutani, B. T., Jones, D. E., Mendis, D. A. 1986, GRL, 13, 287
Spinrad, H., Brown, M. E., Johns, C. M. 1994, AJ, 108(4), 1462
Tozzi, G. P., Feldmann, P. D., Weaver, H. A. 1994, A&A, 285, L9
Voloshina, I. B., Glushneva, I. N., Doroshenko, B. T. et al., 1982, Spektrophotometriya yarkih zvezd, Nauka, Moskow, (russ.)
Wegmann, R., Schmidt, H. U., Huebner, W. F., Boice, D. C. 1987, A&A, 187, 339
Wegmann, R. 1995, A&A, 294, 601
Winnecke, A. 1864, Mém. Acad. Imp. Sci St.-Pétersbourg, 7, 7, 1
Yoshida S., Aoki T., Soyano, T., et al., 1993, PASJ, 45, L33

This article was processed by the author using Springer-Verlag LaTeX A&A style file *L-AA* version 3.